

# Effective Gauge Fields and Topological Band Structures in Pilot-Wave Hydrodynamics

Ethan Andersson and Valeri Frumkin<sup>1</sup>

<sup>1</sup>Department of Mechanical Engineering, Boston University, Boston, Massachusetts, USA

(Dated: December 29, 2025)

We demonstrate that pilot-wave hydrodynamics provides a macroscopic platform for realizing band-structure physics, topological edge states, and gauge-field-induced phase shifts. We show that a submerged square lattice produces frequency-dependent transmission governed by Bloch bands. An inversion-asymmetric honeycomb lattice confines the droplet to a domain wall, revealing a hydrodynamic analogue of a valley-Hall edge state. And a chiral annular structure generates an effective gauge field that produces an Aharonov-Bohm like phase difference between clockwise and counter-clockwise orbits. Unlike conventional wave analogs, pilot-wave hydrodynamics couples a localized particle to its self-generated wave field, providing direct access to topological wave-particle behavior normally associated with quantum systems.

**Introduction.** Topological effects play a foundational role in modern condensed-matter and wave physics, giving rise to protected edge modes in electronic, photonic, and mechanical systems [1–4]. Their controlled experimental realization, however, often relies on technically challenging platforms, such as cryogenic quantum Hall and topological-insulator devices [5], nanofabricated photonic structures [6], or on-chip mechanical and phononic metamaterials operating at MHz frequencies [7], that limit accessibility and hinder the intuitive exploration of the underlying physics. Hydrodynamic analogs, by contrast, offer a macroscopic route to explore topological wave behavior in visually transparent and accessible systems. Surface waves over spatially varying or periodically structured topographies have been shown to obey equations formally equivalent to those governing electromagnetic waves in photonic crystals [8–10]. In the shallow-water regime, the depth  $h(\mathbf{r})$  enters as an effective dielectric parameter, and periodic modulation of  $h(\mathbf{r})$  produces hydrodynamic band structures featuring Dirac-cone degeneracies and symmetry-protected edge states [8, 11]. The underlying operator is mathematically identical to that of a photonic crystal, implying that the full suite of topological phenomena can, in principle, be realized in suitably engineered hydrodynamic systems.

The hydrodynamic *pilot-wave* system [12, 13], discovered by Couder and Fort in 2005 [14], provides a unique setting in which a localized particle (droplet) self-propels across a vibrating liquid surface via resonant interaction with a pilot-wave of its own making. This system has provided the basis for a growing list of hydrodynamic quantum analogs, including single particle diffraction and interference [15], quantization of orbital states [16], the quantum corral [17, 18], the Kapitza-Dirac effect [19], emergent order in spin lattices [20], Bohmian trajectories [21, 22], and Anderson localization [23]. A defining feature of pilot-wave hydrodynamics is the coexistence of a localized particle-like droplet and a delocalized wave field generated by the droplet itself. The droplet's horizontal motion is strictly guided by this self-generated pilot-wave: it can only move along trajectories where the

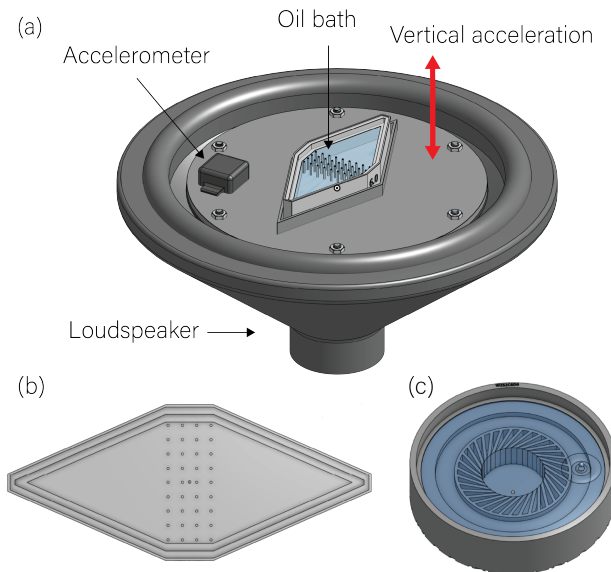


**Figure 1. A schematic illustration of the experimental setup:** (a) A loudspeaker provides harmonic forcing,  $f = \gamma \sin \omega t$  to a circular base plate that holds a small bath of silicon oil with 3D printed topography. (b) A rhombus-shaped bath containing a square lattice of circular pillars of radius  $r = 0.5$  mm, depth  $h = 10$  mm, and lattice constant  $a = 6$  mm, used as a barrier between its two sides. (c) A circular channel 2 mm deep, with inner radius of 18.5 mm and outer diameter of 24.5 mm, enclosing a strip with chiral topography. The well at the center is 8 mm deep and 10 mm in radius.

underlying surface wave can propagate, and is effectively forbidden from entering regions where the pilot-wave amplitude is evanescent [24]. Consequently, one expects that when the droplet encounters a structured environment that acts as a “wave crystal”, the band structure of the pilot-wave imposes corresponding kinematic constraints on the droplet. Thus, in a pilot-wave band gap the droplet is excluded from the crystal, yielding a macroscopic analog of quantum-mechanical band exclusion acting on a particle, rather than the purely wave-based phenomena typical of classical topological platforms.

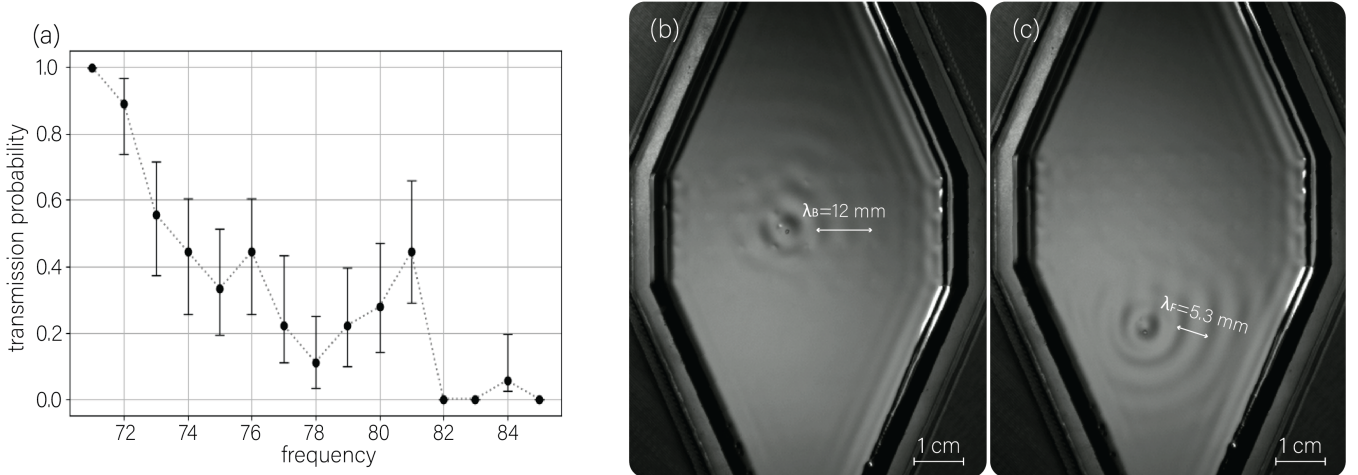


**Figure 2. Band-gap behavior in pilot-wave hydrodynamics:** (a) Transmission probability as a function of driving frequency. At 71 Hz the droplet is transmitted through the lattice; transmission probability drops with an increase in frequency, and starting at 82 Hz, a hydrodynamic band-gap is opened and the droplet is reflected at all times. (b) As the droplet enters a square lattice of circular pillars (radius  $r = 0.5 \text{ mm}$ , lattice constant  $a = 6 \text{ mm}$ ) in the transmission regime ( $f = 71 \text{ Hz}$ ), its pilot wave exhibits a spatially modulated envelope in accordance with Bloch's theorem for waves in periodic media. (c) Outside the lattice, the pilot-wave returns to its unperturbed horseshoe profile.

Motivated by this, we here show that pilot-wave hydrodynamics constitutes a macroscopic platform for realizing topological band structures, edge states, and effective gauge fields within a single, unified framework. By shaping the bath topography, and using the analogy between surface waves and the Bloch eigenproblem of electromagnetic modes in photonic crystals, we experimentally demonstrate the emergence of energy band gaps at selected actuation frequencies, along with topologically protected edge states localized at interfaces between regions of contrasting topography. We then show that introducing chirality into the topography breaks mirror symmetry at the effective level and generates an emergent vector potential that acts on the surface-wave phase, giving rise to an Aharonov–Bohm–like splitting [25, 26] between clockwise and counter-clockwise droplet orbits. These results establish pilot-wave hydrodynamics as a simple, table-top system in which synthetic gauge fields and topological phenomena are realized through the dynamics of a particle guided by its self-generated wave field, in close analogy to quantum mechanics.

**Theory.** The dynamics of the surface elevation  $\eta(\mathbf{r}, t)$  in an inviscid, incompressible, and irrotational fluid of local depth  $h(\mathbf{r})$  are governed, in the linear regime, by

$$\partial_t^2 \eta = \nabla \cdot [g h(\mathbf{r}) \nabla \eta] - \frac{\sigma}{\rho} \nabla \cdot [h(\mathbf{r}) \nabla (\nabla^2 \eta)], \quad (1)$$

where  $g$  is gravity,  $\sigma$  surface tension, and  $\rho$  the density [27]. In the absence of capillarity ( $\sigma = 0$ ), Eq. (1) reduces to the shallow-water wave equation

$$\nabla \cdot [h(\mathbf{r}) \nabla \eta] + \frac{\omega^2}{g} \eta = 0,$$

which is mathematically equivalent to the two-dimensional transverse-magnetic (TM) Maxwell equation

$$\nabla \cdot [\varepsilon^{-1}(\mathbf{r}) \nabla H_z] + \omega^2 \mu(\mathbf{r}) H_z = 0,$$

under the correspondence  $H_z \leftrightarrow \eta$ ,  $\varepsilon^{-1}(\mathbf{r}) \leftrightarrow h(\mathbf{r})$ , and  $\mu(\mathbf{r}) \leftrightarrow 1/g$  [8, 9]. Periodic modulation of  $h(\mathbf{r})$  therefore endows Eq. (1) with a Bloch-band structure directly analogous to that of a photonic crystal [28, 29].

The capillary contribution in Eq. (1) introduces a bi-harmonic term proportional to  $\nabla^4 \eta$ , which has no analogue in local Maxwell theory. This term may be interpreted as a weak, spatially dispersive (nonlocal) correction to the effective dielectric response,

$$\varepsilon_{\text{eff}}^{-1}(\mathbf{r}, \mathbf{k}) = h(\mathbf{r}) [1 + (\sigma/\rho g) k^2],$$

preserving the Bloch-band structure while modifying the high- $k$  dispersion through capillary stiffening.

To describe anisotropic or chiral topographies, we generalize the scalar depth  $h(\mathbf{r})$  to a symmetric second-rank tensor

$$\mathbf{G}(\mathbf{r}) = \begin{pmatrix} G_{xx} & G_{xy} \\ G_{xy} & G_{yy} \end{pmatrix}, \quad (2)$$

which captures the directional dependence of the effective restoring force arising from layered, oblique, or spiral structures. Here  $\mathbf{G}(\mathbf{r})$  serves as the hydrodynamic analog of rotated permittivity tensors in transformation optics [30]. With this substitution, the leading-order gravity term becomes

$$\nabla \cdot [g \mathbf{G}(\mathbf{r}) \nabla \eta].$$

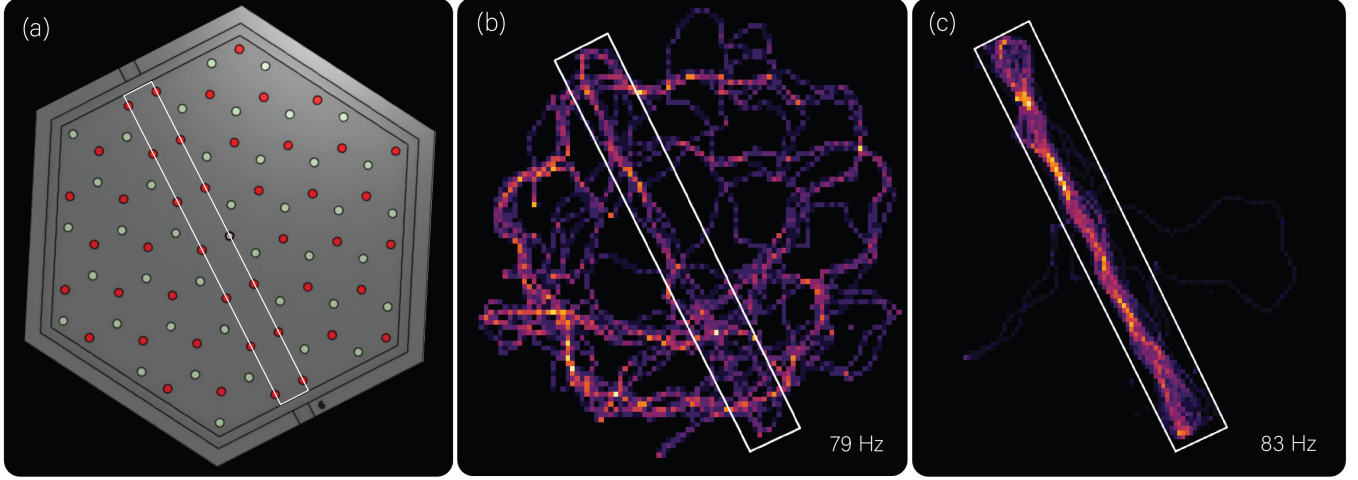


**Figure 3. Topological edge states in pilot-wave hydrodynamics:** (a) A honeycomb lattice of circular pillars of radius  $r = 0.8$  mm, with two pillar heights  $a = 12$  mm and  $b = 13$  mm, corresponding to a controlled modulation of the local depth on the  $A$  and  $B$  sublattices (lattice constant  $c = 12$  mm), producing a 1D interface running along the center of the bath. (b) When driven at frequencies outside the band gap of the bulk honeycomb crystal (here 79 Hz), the droplet is not confined to the interface, exploring the entire lattice. (c) Inside the band gap (here 83 Hz), the droplet does not penetrate into either domain, locking onto the boundary and traveling along it.

Spatial variations of  $\mathbf{G}(\mathbf{r})$  generate first-order derivative terms that can be recast in gauge-covariant form. Writing the operator in divergence form and isolating these contributions yields

$$\nabla \cdot [g \mathbf{G}(\mathbf{r}) \nabla \eta] = g (\nabla - i\mathbf{A}_{\text{eff}}) \cdot \mathbf{G}(\mathbf{r}) (\nabla - i\mathbf{A}_{\text{eff}}) \eta. \quad (3)$$

The explicit form of the emergent vector potential together with its detailed derivation, are given in the Supplemental Material (SM). Equation (3) shows that anisotropic or chiral depth profiles act as synthetic gauge fields for surface waves.

In a ring-like geometry,  $\mathbf{A}_{\text{eff}}$  develops a finite azimuthal component  $A_\theta^{\text{eff}}$ , leading to discrete eigenfrequencies

$$\omega_m^2 = \frac{gh_0}{R^2} (m - \Phi_{\text{eff}})^2; \quad \Phi_{\text{eff}} = \frac{1}{2\pi} \oint_0^{2\pi} A_\theta^{\text{eff}} d\theta, \quad (4)$$

where  $m$  is the azimuthal mode number (see SM). This expression is identical to the spectrum of a charged particle on a ring threaded by magnetic flux due to the Aharonov-Bohm effect [25, 26]. The degeneracy between  $m$  and  $-m$  is lifted whenever  $\Phi_{\text{eff}} \neq 0$ , leading to different frequencies (and hence different velocities) for clockwise and counter-clockwise modes, thus predicting a chirality-dependent velocity of walking droplets orbiting a spiral topography.

*Experiments.* Our experimental setup is depicted in Figure 1. It consists of a shallow bath with 3D-printed topography, mounted on a circular base-plate that is driven vertically by a loudspeaker (Fig. 1a). The bath is filled with silicone oil with surface tension  $\sigma = 0.0209$  N/m, viscosity 20 cSt, and density

$\rho = 0.965 \times 10^{-3}$  kg/m<sup>3</sup>. The experiments are conducted under the Faraday threshold at which the liquid interface destabilized to a pattern of sub-harmonic Faraday waves [31], but above the droplet's walking threshold [14]. In all experiments, we introduced a shallow strip between the topography of interest and the confining walls of the bath, to dampen any oscillations due to the meniscus formed between the oil surface and the confining walls. We visualized the droplet position and pilot-wave using a charge-coupled device camera mounted above a semi-reflective mirror angled at 45° relative to the bath. We then position a diffuse-light source horizontally in front of the mirror, yielding images with bright regions corresponding to extrema or saddle points on the free surface. For the topological edge states experiment, we use side illumination to increase contrast between the droplet and its surroundings, and employed standard Python particle tracking module [32] to track the droplet's trajectory. A detailed description of experimental setup and the precise parameters at which all experiments were conducted, is given in the SM.

We investigated three distinct classes of submerged topographies, each designed to probe a different aspect of topological phenomena in pilot-wave hydrodynamics. The first topography consists of a rhombus-shaped bath whose interior is divided by a submerged wall formed from a square lattice of circular pillars of radius  $r = 0.5$  mm, with spacing of  $a = 6$  mm, and height of 10 mm (Fig. 1b). The rhombus geometry serves to steer the walking droplet away from the corners and toward the submerged barrier, ensuring consistent interaction with the lattice. The overall depth of the bath was  $10.6 \pm 0.15$

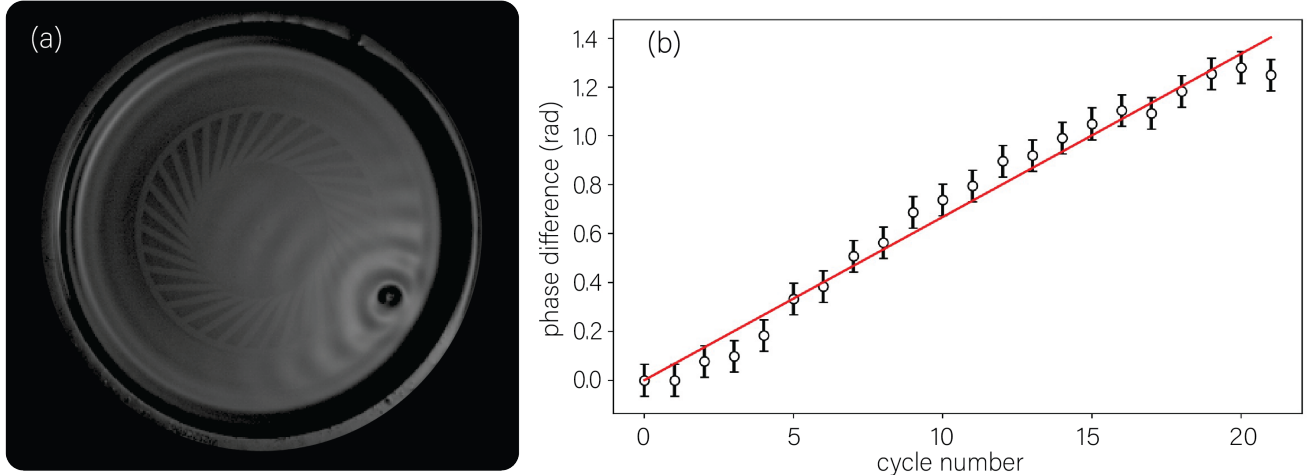


**Figure 4. Geometric phase accumulation in pilot-wave hydrodynamics:** (a) A top view of the experiment showing the skewing of the droplet's pilot-wave by the underlying chiral topography. (b) Accumulative phase difference per cycle between clockwise and counter-clockwise rotations of a droplet circling submerged chiral topography, demonstrating Aharonov-Bohm-like level splitting. An extended measurement of the accumulative phase, showing an excellent linear fit over 40 cycles, is provided in the SM.

mm, so that the pillars were fully submerged under an oil layer of thickness  $0.6 \pm 0.15$  mm.

By varying the driving frequency, we demonstrate that the lattice acts as a frequency-selective waveguide. Figure 2a shows the measured probability of droplet transmission across the submerged lattice as a function of driving frequency: at 71 Hz the droplet crosses the submerged barrier with unit probability (supplemental video 1), while around 82 Hz, the droplet is reflected at all times (supplemental video 2). At intermediate frequencies, transmission probability drops non-monotonically with the increase in frequency. In the transmission regime (Fig. 2b), the droplet's pilot wave exhibits a spatially modulated envelope whose periodicity matches the reciprocal lattice of the submerged pillars ( $\approx 12$  mm), consistent with Bloch's theorem for waves in periodic media. Supplemental video 3 shows a close-up, slow-motion view of the modulation of the droplet's pilot-wave. Outside the lattice, the pilot wave reverts to the familiar horseshoe-shaped profile of the unperturbed walker (Fig. 2c, and supplemental video 1). Together, these observations confirm that the droplet-lattice interaction is mediated through the band structure of the underlying surface-wave field.

The second topography is a honeycomb lattice of circular pillars of radius  $r = 0.8$  mm, with two pillar heights  $a = 12$  mm and  $b = 13$  mm, corresponding to a controlled modulation of the local depth on the  $A$  and  $B$  sublattices (lattice constant  $c = 12$  mm). Two domains with opposite sublattice asymmetry ("lattice" and "anti-lattice") are placed side-by-side, producing a 1D interface running along the center of the bath (Fig. 3a). This

configuration breaks mirror symmetry in opposite ways across the interface and is expected, by analogy with the valley-Hall mechanism, to support symmetry-protected edge states for the surface-wave field. When driven at frequencies outside the band gap of the bulk honeycomb crystal (here 79 Hz), the droplet is not confined to the interface, exploring the entire lattice (Fig. 3b). However, when driven at frequencies inside the band gap of the bulk honeycomb crystal (here 83 Hz), the droplet does not penetrate into either domain, locking onto the boundary and traveling along it (Fig. 3c). This guided motion reflects the presence of a hydrodynamic edge state localized to the interface, analogous to the valley-Hall edge modes of topological photonic and phononic crystals.

The third topography consists of an annular channel containing a chiral arrangement of submerged structures at its center (Fig. 1c). The circular channel was 2 mm deep, with inner radius of 18.5 mm and outer radius of 24.5 mm. The enclosed chiral strip was 8 mm deep and had an inner radius of 10 mm. The spatially varying, mirror-asymmetric depth profile generates an effective gauge field for the surface waves (Fig. 4a), which imparts opposite geometric phases to clockwise and counter-clockwise trajectories. As a result, two droplets orbiting the channel in opposite directions accumulate a measurable phase difference over time (Fig. 4b). This behavior is the hydrodynamic analogue of the Aharonov-Bohm splitting for charged particles encircling a magnetic flux tube, and it directly demonstrates chirality-induced gauge-field control of the walker's orbital dynamics. A recently introduced pilot-wave experiment demonstrates a complementary Aharonov-Bohm analogue in which a droplet orbits

a rotating cylinder that actively generates a surface vortex [33]. In contrast, the gauge-field effects reported here arise passively from chiral topography alone, without any imposed fluid rotation, enabling a purely geometric route to AB-like phase accumulation.

*Discussion.* Our experiments demonstrate that pilot-wave hydrodynamics provides a versatile macroscopic platform for exploring wave phenomena commonly associated with photonic, phononic, and electronic topological systems. In the simplest periodic geometry, the droplet's interaction with a submerged square lattice reveals frequency-selective transmission and reflection that are controlled by the Bloch band structure of the underlying surface-wave field. In the inversion-asymmetric honeycomb lattice, we observe edge-guided transport analogous to the valley-Hall mechanism. Here the droplet's pilot wave inherits the topological character of the bulk band structure, confining its motion to a one-dimensional interface between regions of opposite sublattice asymmetry. The chiral annular geometry further extends this connection by demonstrating a hydrodynamic analogue of the Aharonov-Bohm effect. The mirror-asymmetric topography induces an effective gauge field for the surface-wave phase, resulting in a measurable splitting between clockwise and counter-clockwise orbits.

Notably, because the walker couples a coherent wave field to a localized particle, the system enables simultaneous access to the wave-based origins of topological phenomena and their particle-level manifestations. This dual character suggests new directions for studying wave-particle analogs of quantum transport, synthetic fields, and topological control in a simple table-top environment, and points to the broader potential of hydrodynamic systems as accessible testbeds for emergent geometric and topological physics.

ties in a semiconductor photonic crystal platform [Invited]. *Optical Materials Express*, 11(2):319–337, February 2021. Publisher: Optica Publishing Group.

- [7] Jinwoong Cha, Kun Woo Kim, and Chiara Daraio. Experimental realization of on-chip topological nanoelectromechanical metamaterials. *Nature*, 564(7735):229–233, December 2018. Publisher: Nature Publishing Group.
- [8] Huanyang Chen, Jiong Yang, Jian Zi, and C. T. Chan. Transformation media for linear liquid surface waves. *EPL*, 85(2):24004, January 2009. Publisher: EDP Sciences.
- [9] Shan Zhu, Xinyu Zhao, Linkang Han, Jian Zi, Xinhua Hu, and Huanyang Chen. Controlling water waves with artificial structures. *Nature Reviews Physics*, 6(4):231–245, April 2024. Publisher: Nature Publishing Group.
- [10] Bo Wang, Zhiyuan Che, Cheng Cheng, Caili Tong, Lei Shi, Yijie Shen, Konstantin Y. Bliokh, and Jian Zi. Topological water-wave structures manipulating particles. *Nature*, 638(8050):394–400, February 2025. Publisher: Nature Publishing Group.
- [11] Jiuyang Lu, Chunyin Qiu, Shengjun Xu, Yangtao Ye, Manzhu Ke, and Zhengyou Liu. Dirac cones in two-dimensional artificial crystals for classical waves. *Physical Review B*, 89(13):134302, April 2014. Publisher: American Physical Society.
- [12] John W. M. Bush and Anand U. Oza. Hydrodynamic quantum analogs. *Reports on Progress in Physics*, 84(1):017001, 2020.
- [13] John W. M. Bush, Valeri Frumkin, and Pedro J. Sáenz. Perspectives on pilot-wave hydrodynamics. *Applied Physics Letters*, 125(3):030503, July 2024.
- [14] Y. Couder, S. Protière, E. Fort, and A. Boudaoud. Walking and orbiting droplets. *Nature*, 437(7056), 2005.
- [15] Yves Couder and Emmanuel Fort. Single-Particle Diffraction and Interference at a Macroscopic Scale. *Physical Review Letters*, 97(15):154101, October 2006. Publisher: American Physical Society.
- [16] Emmanuel Fort, Antonin Eddi, Arezki Boudaoud, Julien Moukhtar, and Yves Couder. Path-memory induced quantization of classical orbits. *Proceedings of the National Academy of Sciences*, 107(41), 2010.
- [17] Daniel M. Harris, Julien Moukhtar, Emmanuel Fort, Yves Couder, and John W. M. Bush. Wavelike statistics from pilot-wave dynamics in a circular corral. *Physical Review E*, 88(1):011001, 2013.
- [18] Pedro J. Sáenz, Tudor Cristea-Platon, and John W. M. Bush. Statistical projection effects in a hydrodynamic pilot-wave system. *Nature Physics*, 14(3), 2018.
- [19] Bauyrzhan K. Primkulov, Davis J. Evans, Valeri Frumkin, Pedro J. Sáenz, and John W. M. Bush. Diffraction of walking drops by a standing Faraday wave. *Physical Review Research*, 7(1):013226, February 2025. Publisher: American Physical Society.
- [20] Pedro J. Sáenz, Giuseppe Pucci, Sam E. Turton, Alexis Goujon, Rodolfo R. Rosales, Jörn Dunkel, and John W. M. Bush. Emergent order in hydrodynamic spin lattices. *Nature*, 596(7870), 2021.
- [21] Valeri Frumkin, David Darrow, John W. M. Bush, and Ward Struyve. Real surreal trajectories in pilot-wave hydrodynamics. *Physical Review A*, 106(1):L010203, July 2022.
- [22] Valeri Frumkin and John W. M. Bush. Misinference of interaction-free measurement from a classical sys-

---

- [1] M. Z. Hasan and C. L. Kane. Colloquium: Topological insulators. *Reviews of Modern Physics*, 82(4):3045–3067, November 2010. Publisher: American Physical Society.
- [2] Xiao-Liang Qi and Shou-Cheng Zhang. Topological insulators and superconductors. *Reviews of Modern Physics*, 83(4):1057–1110, October 2011. Publisher: American Physical Society.
- [3] Ling Lu, John D. Joannopoulos, and Marin Soljačić. Topological photonics. *Nature Photonics*, 8(11):821–829, November 2014. Publisher: Nature Publishing Group.
- [4] Sebastian D. Huber. Topological mechanics. *Nature Physics*, 12(7):621–623, July 2016. Publisher: Nature Publishing Group.
- [5] Electrical and superconducting transport in topological insulator nanoribbons. In *Frontiers of Nanoscience*, volume 20, pages 241–264. Elsevier, January 2021. ISSN: 1876-2778.
- [6] Satoshi Iwamoto, Yasutomo Ota, and Yasuhiko Arakawa. Recent progress in topological waveguides and nanocav-

tem. *Physical Review A*, 108(6):L060201, December 2023. Publisher: American Physical Society.

[23] Abel J. Abraham, Stepan Malkov, Frane A. Ljubetic, Matthew Durey, and Pedro J. Sáenz. Anderson Localization of Walking Droplets. *Physical Review X*, 14(3):031047, September 2024. Publisher: American Physical Society.

[24] Giuseppe Pucci, Pedro J. Sáenz, Luiz M. Faria, and John W. M. Bush. Non-specular reflection of walking droplets. *Journal of Fluid Mechanics*, 804:R3, October 2016.

[25] Y. Aharonov and D. Bohm. Significance of Electromagnetic Potentials in the Quantum Theory. *Physical Review*, 115(3):485–491, August 1959. Publisher: American Physical Society.

[26] Akira Tonomura, Tsuyoshi Matsuda, Ryo Suzuki, Akira Fukuhara, Nobuyuki Osakabe, Hiroshi Umezaki, Junji Endo, Kohsei Shinagawa, Yutaka Sugita, and Hideo Fujifara. Observation of Aharonov-Bohm Effect by Electron Holography. *Physical Review Letters*, 48(21):1443–1446, May 1982. Publisher: American Physical Society.

[27] Horace Lamb and Sir Horace Lamb. *Hydrodynamics*. Cambridge University Press, November 1993. Google-Books-ID: 2grlAQAAQAAJ.

[28] Nicolas Laforge, Vincent Laude, Franck Chollet, Abdelkrim Khelif, Muamer Kadic, Yuning Guo, and Roman Fleury. Observation of topological gravity-capillary waves in a water wave crystal. *New Journal of Physics*, 21(8):083031, August 2019. Publisher: IOP Publishing.

[29] Mehul P. Makwana, Nicolas Laforge, Richard V. Craster, Guillaume Dupont, Sébastien Guenneau, Vincent Laude, and Muamer Kadic. Experimental observations of topologically guided water waves within non-hexagonal structures. *Applied Physics Letters*, 116(13):131603, April 2020.

[30] J. B. Pendry, D. Schurig, and D. R. Smith. Controlling Electromagnetic Fields. *Science*, 312(5781):1780–1782, June 2006. Publisher: American Association for the Advancement of Science.

[31] Michael Faraday. XVII. On a peculiar class of acoustical figures; and on certain forms assumed by groups of particles upon vibrating elastic surfaces. *Philosophical Transactions of the Royal Society of London*, (121):299–340, December 1831.

[32] John C. Crocker and David G. Grier. Methods of Digital Video Microscopy for Colloidal Studies. *Journal of Colloid and Interface Science*, 179(1):298–310, April 1996.

[33] Georgi Gary Rozenman, Kyle I. McKee, Arnaud Lazarus, Valeri Frumkin, and John W. M. Bush. Observation of the Aharonov-Bohm Effect in Pilot-Wave Hydrodynamics, December 2025. arXiv:2512.21263 [physics].